Characterization of Single-Photon Time Resolution: From Single SPAD to Silicon Photomultiplier

Fabio Acerbi, *Member, IEEE*, Alessandro Ferri, Alberto Gola, *Member, IEEE*, Massimo Cazzanelli, Lorenzo Pavesi, *Senior Member, IEEE*, Nicola Zorzi, and Claudio Piemonte, *Member, IEEE*

Abstract—In this paper, we report on the characterization of the single-photon time resolution (SPTR) of the RGB (Red-Green-Blue) type silicon photomultipliers (SiPM) produced at FBK. We measured and compared single-photon timing jitter of 1×1 mm^2 and 3×3 mm^2 SiPMs, and also of square SPADs with integrated passive quenching, identical to the cells composing the SiPMs. We reached a single-photon time resolution of about 180 ps full-width at half-maximum for 3×3 mm^2 SiPM, 80 ps for 1×1 mm^2 SiPM and less than 50 ps for single cells. From measurements with pin-holes placed in front of 1×1 mm^2 detector we see a very good cell-to-cell uniformity: it is not a limiting factor for time resolution. We also characterized the timing jitter of SiPMs as a function of the number of photons per laser pulse (N) finding that it does not decrease exactly with the square root of N because of the optical crosstalk between cells.

Index Terms—Photodetector, photon timing, silicon photomultiplier, single photon, SiPM, TCSPC, time resolution.

I. INTRODUCTION

SILICON PHOTOMULTIPLIERS (SiPMs) have obtained a growing attention as an alternative to the traditional photomultiplier tubes in applications based on detection of low photon fluxes thanks to a number of advantages such as compactness, ruggedness, ease of use, low operational voltage and insensitivity to magnetic fields [1].

SiPMs can be also successfully used in applications where efficient and fast detection of scintillation light is required, e.g. in nuclear medicine and high-energy physics. For example it allows important advancements in the field of positron emission tomography (PET) where its small size and insensitivity to magnetic fields allow a compact packing and the combination with magnetic resonance imaging (MRI) [2], whilst its very good time resolution allows time of flight (TOF) PET, which improves image quality [3], [4], [5].

The single-photon time resolution (SPTR), i.e. timing jitter measured when one photon is being detected, is an important feature of silicon photomultipliers and it is important in many applications: i) it has a direct influence on the best achievable time resolution of time-of-flight detectors when used in high-energy and medical physics (with scintillators) [6], [7] and ii) it is very important in all the applications based on low-light detection, e.g. the readout of Cherenkov radiators [8], [9], [10] (between tens to hundreds of photoelectrons per pulse). Photomultiplier tubes (PMT) have typically a SPTR between few hundreds of picoseconds (e.g. 270 ps [11]) and few nanoseconds. However, best multi-channel plate photomultiplier tubes (MCP-PMTs) reach a SPTR of about $\sigma = 30$-50 ps, and the SPTR of silicon photomultipliers has been usually slightly worse [8].

A SiPM is basically made of many single-photon avalanche diodes (SPADs), each with a quenching resistor lithographically fabricated close to it, and connected to a common top-contact. The overall performance of SiPMs is strongly dependent on the uniformity of single cells (i.e. the single passively-quenched SPADs) characteristics, in particular the timing response is given by the superposition of all single-cell responses. Moreover, previous work showed how in SiPMs with big area, there could be significant difference in timing response between the pixels near the bonding pad and the furthest ones [12], due to differences in trace impedance (between cell and bonding pad).

In this paper we characterized the single photon time resolution of 1×1 mm^2 and 3×3 mm^2 silicon photomultipliers produced at FBK at different bias conditions and at two different wavelengths. In order to understand which are the limiting factors of the SPTR we characterized and compared the timing performance of the SiPMs with a square SPAD identical to the single cell of the silicon photomultipliers (from the same wafer). In addition we checked the influence of pixel position and parasitics employing a pinhole in front of the SiPM, illuminating only a small portion or a single cell. Finally, we characterized the dependence of timing jitter of SiPMs on the number of photons per laser pulse.

II. DEVICE CHARACTERISTICS

The typical cross-section of the tested SiPMs is shown in Fig. 1: each cell is made of n-on-p implants on a p^- epitaxial layer grown on a p^{++} substrate. A quenching resistor connects the n-implant of each cell to the common metal grid on the top and there is a common metallization on the back of the chip. The deep implant defines the active area of the cell.

We tested 1×1 mm^2 and 3×3 mm^2 SiPMs and a square SPADs identical to their single cell. They were all taken from
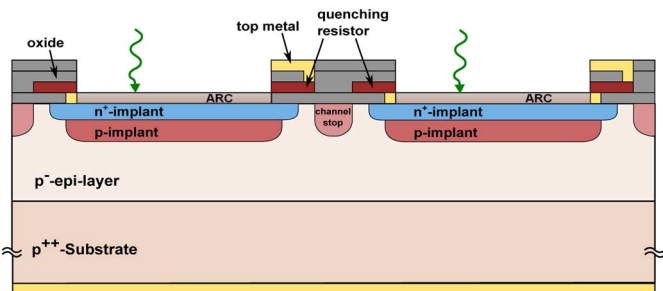
Fig. 1. SiPM cross-section (n-on-p technology) showing the structure of the cells. The deep implant defines cell's active area.

Fig. 2. Dark count rate, (primary and total), measured at $20\,^{\circ}$C, as a function of excess bias, of 1×1 mm^2 and 3×3 mm^2 SiPMs.

the same wafer, from a new FBK production run (identified as #1), in which we were able to achieve a remarkable low noise (in terms of primary dark count rate, DCR).

To have a comparison with other devices, and to study the influence of the DCR we also tested other two 1×1 mm^2 SiPMs and another 50-μm cell from older production runs (#2 and #3), with the same cell layout and fabrication process but with higher primary noise (#3 devices selected to have very high DCR). Performance of SiPM #2 is described in [13].

A. Detection Efficiency and Dark Count Rate

We characterized the Photon Detection Efficiency (PDE) of 1×1 mm^2 SiPM from production run #2, as a function of wavelength, at room temperature. The fill factor is about 45%. We employed a setup composed by a broad-spectrum light source, optical neutral filters and a monochromator, whose light was focused into active area of the Device Under Test (DUT). A calibrated reference detector was positioned in place of the DUT to characterize the system and then primary count rate of the SiPM has been measured (afterpulsing and crosstalk have been excluded), with and without light, subtracting the dark count rate from the measured count rate with light. We check also the PDE of 1×1 mm^2 SiPM from production run #1 in several points of the spectrum obtaining similar (but slightly lower) results.

For both PDE and dark count rate measurements we employed the procedure described in [14] for the discrimination of primary counts from the correlated noise components: we recorded milliseconds long output waveforms with the oscilloscope and built amplitude vs. inter-arrival time plot, from which it is possible to evaluate the primary, Poisson-distributed DCR, the afterpulsing probability and the cross talk probability.

The measured PDE tops in the blue and green wavelength region (see the PDE curve in [13]). We measured a PDE of 26%, with 2.5 V of excess bias, and of 33% with 6.5 V, at $\lambda = 570$ nm. With 6.5 V of excess bias the PDE is about 22% at $\lambda = 425$ nm and $\sim 9\%$ at $\lambda = 850$ nm.

The dark count rate (DCR) of the SiPMs and single cells were measured at a temperature of $20\,^{\circ}$C, at different bias conditions. Fig. 2 reports the total (with correlated noise) and only primary DCR. Devices from production run #1 have a very low DCR (among lowest ever reported in literature [15]) of about $3.7 \cdot 10^4$ cps/mm^2 (counts per second in a 1-mm^2 device) with 2 V of excess bias and of $\sim 1 \cdot 10^5$ cps/mm^2 at 6 V of excess bias. On

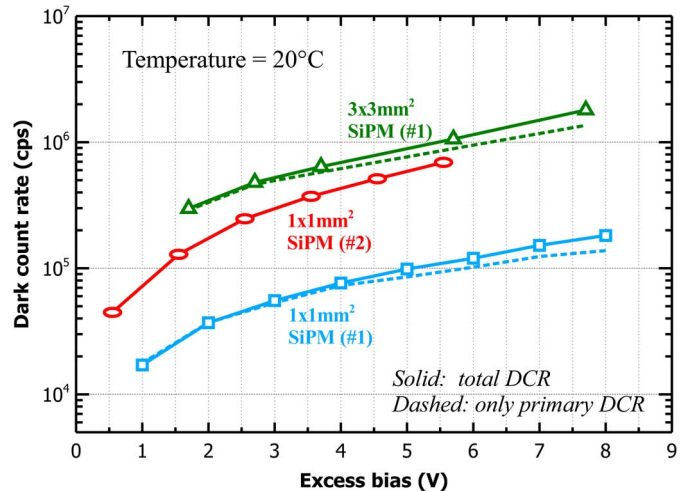the 50-μm square SPAD we measured a remarkably low DCR of about 30 cps at 6 V of excess bias.

The SiPM from production run #2 shows a slightly higher noise, about $1.6 \cdot 10^5$ cps/mm^2 at 2 V of excess bias and about $5 \cdot 10^5$ cps/mm^2 at 5 V, which is still a low value for silicon photomultipliers [15]. Finally, the devices from run #3 show a higher noise, more than two orders of magnitude than the others. In our analysis this characteristic has been useful to check the effect of DCR on time resolution.

III. MEASUREMENT OF TIMING JITTER

The timing jitter measurements were performed illuminating the devices at a single photon level with ultra-short laser-pulses, and measuring the arrival-time jitter of amplified electric signal coming out from the front-end circuit.

A. Setup

As represented in Fig. 3, we employed a mode-locked Ti:Sapphire laser, pumped by a continuous-wave green laser, providing pulses at $\lambda = 850$ nm, with a temporal width of about 2 ps FWHM (Full-Width at Half Maximum) and a repetition rate of 82 MHz. Pulse shape was always controlled by means of the autocorrelator. Since this frequency is higher or comparable with the typical recharge time of tested detectors, we used a pulse-picker. This block is synchronized with the laser and periodically selects one optical pulse over N and blocks the others (extinction ratio of about 1/100). We select optical pulses with a frequency from hundreds of Hertz to few kilohertz. This block also integrates a second harmonic generator, allowing us to measure the timing jitter in the blue-wavelength region ($\lambda = 425$ nm). The output light spot has a diameter of about 1.5 mm, thus, to uniformly spread the light over the SiPM, we used an optical diffuser.

The optical signal is attenuated to a single-photon level by reflective neutral-density filters and sent to the DUT, which is connected to the front-end circuit (based on one AD8000 amplifier in trans-impedance configuration). The amplified electric signal, along with the reference trigger signal are fed to the
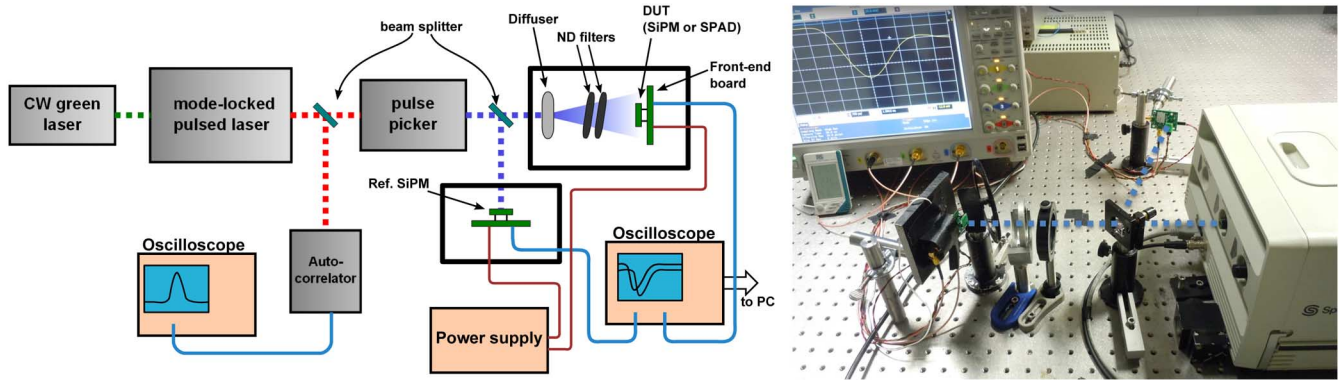
Fig. 3. Schematic representation and photograph of the setup employed for timing jitter measurements.

large-bandwidth (1 GHz), high sampling-rate (20GSample/sec) Agilent oscilloscope, which acquires, digitizes and send them to the PC. For every pair of acquired SiPM and reference signal, a LABVIEW program computes the time distance between the reference and the SiPM signal, using a leading edge discrimination (LED), at several threshold levels on the SiPM signal, and then the arrival-time statistics, thus the timing jitter measurements. The software includes a real-time low-pass filter (principally to reduce the sampling noise) and the extraction of the timing-response curves at different thresholds.

It must be considered that a very precise synchronization signal is mandatory for this kind of jitter measurement, locked with the optical pulses. We performed preliminary system characterizations exploiting the electrical SYNC OUT from the laser, obtaining a minimum resolution of few tens of picoseconds. To lower this limit, we exploited the optical signal itself, splitting it into two paths. A first one, non-attenuated, is sent to a "Reference" SiPM and the second one hits the DUT. To quantify the minimum overall system resolution (i.e. contributions from the detectors, the front-end circuitry and the oscilloscope acquisition and digitalization circuits) we measured the timing jitter between the output signal of two identical SiPMs (both optical paths without filters), obtaining a coincidence time resolution (CTR) of less than 10 ps FWHM. This means a trigger jitter of less than 7 ps $\pm$ 1.2 ps FWHM (quadrature subtraction).

The measurements were performed at room temperature ($\sim$ 24°C), with detectors placed in optically-isolated boxes. Timing jitter values reported in this paper are not deconvoluted from the intrinsic time resolution of the system.

B. Photon Number Discrimination

To measure the timing jitter of the single-cell, we attenuated light-pulses to single-photon level, obtaining a detection rate, at the highest excess bias, which was lower than 1% of the light-pulse rate. This ensures that the probability of a two-photon event is sufficiently low to avoid distortion of the timing response curve.

Conversely, with the SiPM (uniformly illuminated), two measurements methods are possible to quantify the SPTR: i) light can be attenuated to a single-photon level, as for SPAD (thus a SiPM overall detection probability of 1%), but this would result in a very low optical power and long time to collect the
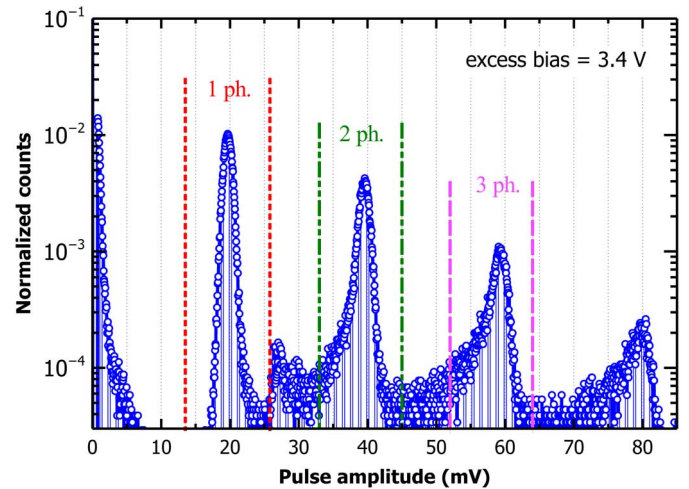

Fig. 4. Histogram of pulse amplitude (after transimpedance amplification, with gain Z $=$ 1000 V/A) of 1 $\times$ 1 mm^2 SiPM at 3.4 V of excess bias, with the representation of the intervals used to discriminate the 1-photon, 2-photons and 3-photons events for the timing jitter measurements.

events, or ii) light can be attenuated to a few-photon level (e.g. 2 average photons per pulse). In such second way, the detection probability of the single cell will be again lower than 1%, but the one-photon events has to be distinguished from the two, three or four photon ones. A similar method has been employed in a previous work [10].

Therefore, for the SPAD, we histogram the difference between the detector and the reference pulse arrival times, whereas, for the SiPM, we first discriminate the events with 1-, 2- or 3-photon pulse amplitude, and then we build three groups of histograms of the arrival time differences, obtaining timing jitters of the SiPM in response to one, two or three photons. An example of pulse amplitude spectrum is shown in Fig. 4: peaks are clearly visible and distinguishable thanks to the low SiPM DCR and afterpulsing, which typically reduce the peak to valley ratio. The peak near 0 represents the events when no avalanche was triggered and the small peak between 1-ph and 2-ph peaks could be caused by the non-perfect suppression of the pulse-picker (the ratio between its amplitude and the 1-ph peak one, equals the extinction ratio).

For each photon number, we build the timing response histograms for each threshold. As an example, Fig. 5 shows the
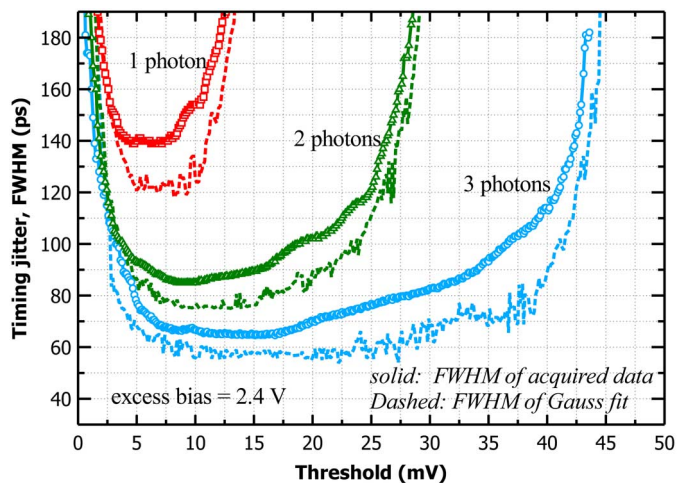
This article has been accepted for inclusion in a future issue of this journal. Content is final as presented, with the exception of pagination.

4   IEEE TRANSACTIONS ON NUCLEAR SCIENCE

Fig. 5. Timing jitter FWHM (1×1 mm^2 SiPM #1) acquired discriminating events with 1, 2, or 3 photons per laser pulse, as a function of the threshold voltage used on front-end amplified output signal. Solid lines are FWHM of acquired histogram; dashed lines represent FWHM of the Gaussian fits.
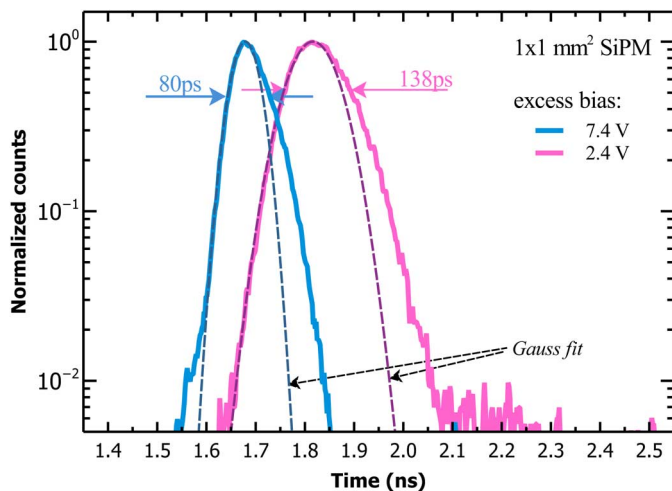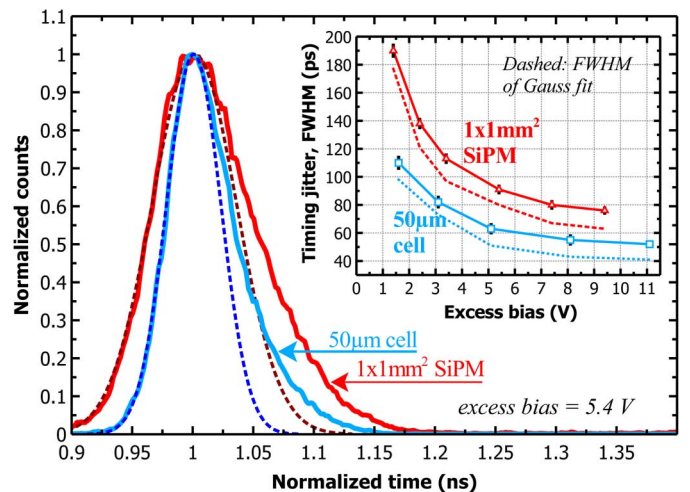

Fig. 7. Comparison between single-photon timing response of the single cell and of the 1×1 mm^2 SiPM #1. The inset reports the timing jitter of both detectors as a function of excess bias (dashed lines are FWHM of the Gaussian fits).

Fig. 6. Single-photon timing response of a 1×1 mm^2 SiPM #1 at two excess biases ($\lambda = 425$ nm).

1-photon, 2-photons and 3-photons curves of the timing jitter (Full-Width at Half-Maximum, FWHM) as a function of the threshold voltage, with 2.4 V of excess bias. Dashed lines are the FWHM of the Gaussian fit on the curve, which usually are narrower due to the tail after main peak in the timing response (see examples in Fig. 6). Jitter deteriorates for low and high threshold: in the first case the threshold is within the electronic noise, in the second because the slope in pulse shape reduces. At the end of each measurement, we considered the minimum values of the 1-photon curve as the timing jitters (or SPTR), used in the timing-jitter vs. bias plots.

IV. Single-Photon Time Resolution

A. Measurements at $\lambda = 425$ nm

We measured the single-photon time resolution of 1×1 mm^2 SiPM at wavelength of 425 nm at different excess biases. As shown in Fig. 6 the timing histograms are very sharp (i.e.

without long tails or second peaks), also when plotted in logarithmic scale. The timing jitter FWHM is about 140 ± 3 ps at 2.4 V of excess bias and it reduces to 80 ± 2 ps at 7.4 V. In the figure, the dashed lines are Gaussian fits that consider mainly the left side of the histogram. Indeed, generally, the single-photon timing response of a SPAD, as well as of a SiPM, is made of a main peak followed by a tail, which is typically due to carriers absorbed in the neutral region, which have to diffuse towards the active area to trigger an avalanche (at times more delayed) [16]. However, in this case, the tail is very small and does not change with excess bias.

Note that unless otherwise specified, the timing jitter reported are extracted from the raw data.

Expressing the SPTR as σ (to compare with other works) we obtain a value of about 34 ps, at 7.4 V of excess bias, which is comparable with the best MCP-PMTs [8].

To investigate the limiting factors of the measured SiPM timing resolution, we first characterized the timing jitter of a square 50-μm side SPAD identical to a single SiPM cell, from the same wafer. The comparison between the single-photon timing responses of the two devices is shown in Fig. 7. It can be noted that the two shapes are similar; there are no additional tails or enlargements on the right part of the SiPM response which could indicate cell-to-cell non-uniformity (e.g. different electric fields or breakdown voltages).

The timing jitter of the single cell is about 80 ± 2.5 ps FWHM at 3 V of excess bias and it reduces to $\sim 50 \pm 2$ ps FWHM at higher voltages.

The higher SPTR of SiPM could be due to: i) a non-uniform behavior of the cells, i.e. either differences in performances or a different path length between cell and bonding pad (which gives different peaking time), ii) higher capacitances and parasitic inductances, which would give a slower signal with lower amplitude, iii) higher baseline fluctuation in the SiPM due to the higher overall dark count rate, which reflects on a pulse amplitude and a threshold crossing-time spread.

To investigate these aspects, we characterized also the timing jitter of a larger silicon photomultiplier with 3×3 mm^2 area.
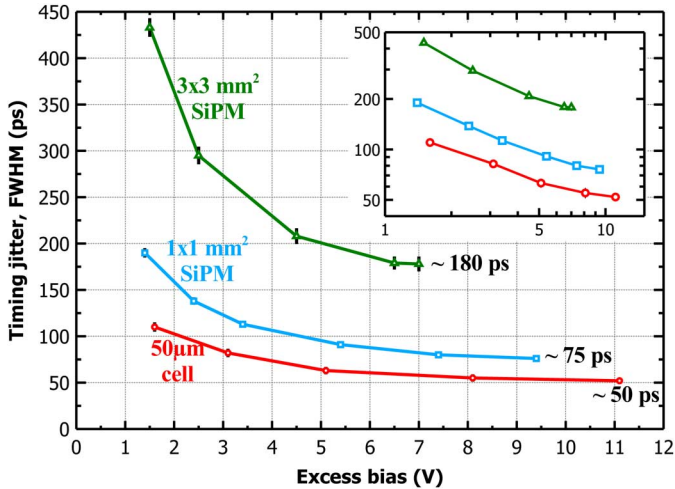
This article has been accepted for inclusion in a future issue of this journal. Content is final as presented, with the exception of pagination.

ACERBI *et al.*: CHARACTERIZATION OF SINGLE-PHOTON TIME RESOLUTION: FROM SINGLE SPAD TO SILICON PHOTOMULTIPLIER 5

Fig. 8. Timing jitter as a function of the excess bias ($\lambda = 425$ nm), measured on 1×1 mm^2 SiPM, 3×3 mm^2 SiPM and 50-μm square cell (production run #1). The inset shows the same curves but in a log-log plot. Error bars represent the standard deviation of the estimated jitter uncertainty (due to minimum bin width and Poisson statistics in timing histograms).

Fig. 9. Average 1-photon voltage pulses (after transimpedance amplification $Z = 1000$ V/A) measured with 50 μm cell, 1×1 mm^2 and 3×3 mm^2 SiPMs. The inset shows the pulse peak-amplitudes as a function of the excess bias.

With such big area, it is generally very difficult to measure the single-photon time-resolution, because of the dark count rate that makes the baseline fluctuation very important (as in old devices characterized in [17]). Instead, in our case, production run #1 has low DCR.

The timing jitter at different excess biases is reported in Fig. 8: for 3×3 mm^2 SiPM we obtained a SPTR of $\sim 180 \pm 9$ ps FWHM at 6.5 V of excess bias, which is about 100 ps higher than 1×1 mm^2 SiPM and ~ 130 ps higher than single cell. Interestingly, when plotting the curves in log-log axis (inset of the figure) they are almost proportional to each other (particularly at low excess bias voltages), progressively shifted to upper values.

The SPTR measured for both SiPMs are among the lowest presented in literature [7], [10], [17], [21].

In a SiPM, as a first approximation, the spread in threshold crossing time (σ_t) (i.e. the timing jitter) is proportional to the amplitude of baseline fluctuation and electronic noise (σ_a) and inversely to the slope of the rising edge of the pulse at the threshold crossing point (f'_{th}) [18], [19], thus:

$$\sigma_t = \frac{\sigma_a}{f'_{th}}$$

Thus, with a given electronic noise, the higher is the pulse amplitude, the greater is the slope and the lower is the timing jitter (when the single-cell "intrinsic" time resolution and the system resolution, are not limiting factors [20]).

We acquired the average single-photon pulses of the three detectors, reported in Fig. 9 (oscillations in the single-cell signal are due to a slight non-stability of the amplifier, but do not affect the validity of the following considerations). In the inset of the figure, we show the pulse peak-amplitude as a function of excess bias. It can be noted that the larger the detector, the slower is the single-cell output signal. This is mainly due to the bigger metal-grid capacitance that introduces a low-pass filtering.

By analyzing the signals acquired with the oscilloscope we checked that the effect of previous dark counts (i.e. fluctuations
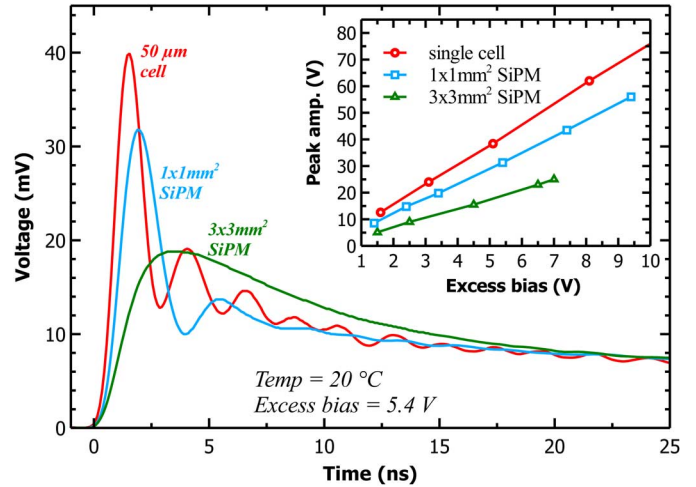
of the baseline due to the slow tail of the signal) is negligible for the single cell and it starts to be important in 1×1 mm^2 SiPM at excess biases higher than about 8.5 V and in 3×3 mm^2 SiPM at excess biases higher than about 6.5 V.

To quantify the contribution of electronic noise on timing jitter, we calculated the sigma of such noise and the rising-edge slope for the three devices. The standard deviation of the electronic noise is between 550 μV and 750 μV (at biases lower than 7 V), whereas, for example, at 5 V the slope of the signals (measured around the best threshold voltage point) are 44 V/μs, 26 V/μs and 9.6 V/μs, respectively for the single cell, the 1×1 mm^2 and the 3×3 mm^2 SiPMs. The estimated electronic-noise contribution (FWHM) to SPTR is ~ 30 ps, ~ 70 ps and ~ 180 ps. This trend is quite in agreement with the measured SPTR (i.e. 60 ps, 90 ps and 195 ps) and the width of the Gaussian fittings (i.e. 51 ps, 80 ps, and 190 ps). Performing this analysis for all the excess biases, we obtained the curves of noise contribution on SPTR, shows in Fig. 10 (3×3 mm^2 SiPM is not reported for better clarity of the plot). Moreover, by deconvolving measured data from noise contribution, we obtained an estimation of the "intrinsic" single-cell SPTR, i.e. the low limit given by statistic process related to avalanche build-up in the single SPAD. As reported in the inset, the value obtained for the three devices are well in agreement and follow the same trend.

In the 50 μm cell, the SPTR equals the intrinsic time resolution, at excess bias greater than about 4 V, whereas in 1×1 mm^2 SiPM, the noise contribution and the intrinsic time resolution are comparable. In 3×3 mm^2 SiPM, instead, the SPTR is entirely dominated by the effect of electronic noise.

Therefore, it can be concluded that a first important aspect that worsens the SPTR of SiPM (with respect to the single cell) is the slower output signal due to the bigger parasitics. This seems to be the main limiting factor in SiPM with a low dark count rate like the one we tested from production run #1, but the effect of dark count on baseline fluctuation could also be important in devices with higher noise.

As a further comparison, we characterized other two 1×1 mm^2 SiPMs and another 50 μm cell from older production

This article has been accepted for inclusion in a future issue of this journal. Content is final as presented, with the exception of pagination.

6   IEEE TRANSACTIONS ON NUCLEAR SCIENCE
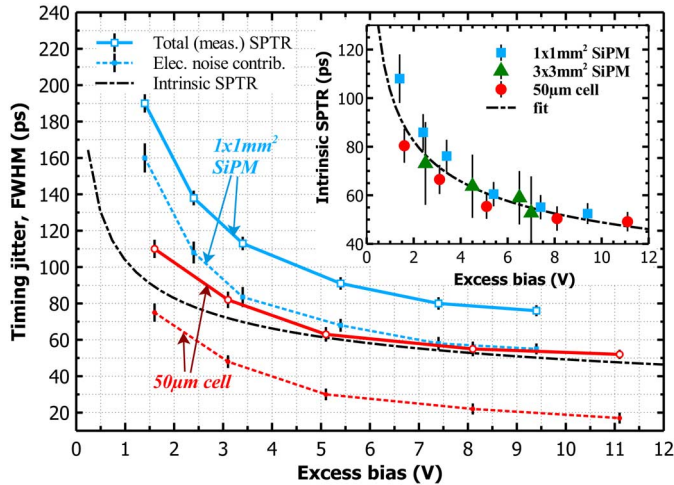

Fig. 10. Estimated contribution of electronic noise to SPTR (dashed lines) compared with measured overall SPTR (FWHM) (solid lines) and estimated "intrinsic" cell SPTR. The inset shows the intrinsic SPTR for the three devices and the fit on all points.
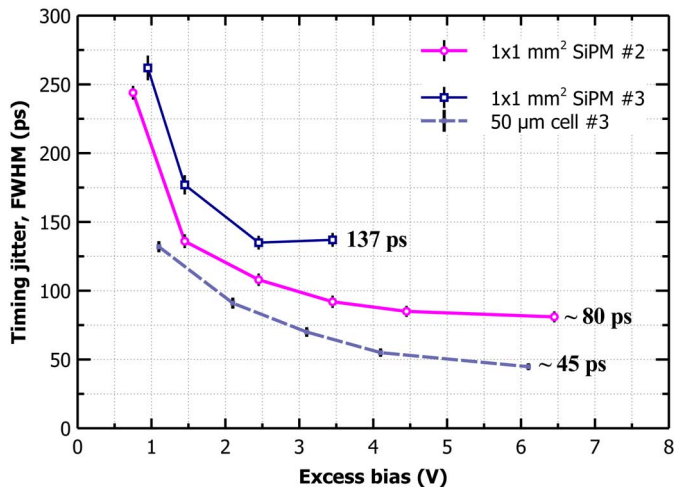

Fig. 11. Timing jitter FWHM as a function of the excess bias ($\lambda = 425$ nm), measured on 1×1 mm^2 SiPM from production run #2, and of 1×1 mm^2 SiPM and $50\ \mu$m square cell from production run #3. Error bars represent the standard deviation of the estimated FWHM uncertainty.

runs, with higher DCR. As shown in Fig. 11, the lowest time resolution measured with SiPM #2 is around 80 ± 2.5 ps at ~ 7 V of excess bias whereas the single cell #3 reaches a timing jitter of $\sim 45 \pm 2$ ps at 6 V of excess bias. These results are quite similar to what was obtained with SiPM and single cell of the new production run. Instead, the timing jitter curve of SiPM #3 saturates already at 2.5 V, at about 140 ps. The main feature of production #3 is the higher dark count rate. This high noise has a moderate effect on the single cell, whereas on the 1×1 mm^2 SiPM it becomes very important and it seems to have a considerable impact on timing performances.

We acquired the pulse-amplitude spectrum for the single cell #3 and we saw a main peak, as expected, similarly to single cell #1, but with an additional tail towards lower amplitudes, which is caused by laser-triggered avalanches happening just after a dark-triggered avalanche, when the detector is not fully recharged yet. When we measured again the timing jitter on

single cell, taking into account only events with full-amplitude pulses, discarding the others, we obtained timing jitter value, at 6 V of excess bias, of about 37 ± 2 ps (about 8 ps less). The better time resolution obtained with single cell #3, compared to single cell #1 (i.e. 37 ps compared to 50 ps) could be due to a slightly different electric field profile in the production runs, which is more evident in single cell thanks to the low timing jitter.

On the SiPM the higher dark count rate has an important effect on timing performance for two reasons: i) a higher fluctuation of the baseline, due to the relatively long tail (recharge part) of the single-cell signal, and ii) a high spread in pulse amplitude. The former could be partially mitigated with tail-cancellation techniques (or front-ends) [18] and the latter by discriminating the amplitudes, but not completely. Both effects, as explained above, worsen timing performance of SiPM #3.

B. Measurements with Pinhole

To analyze the last possible contribution to SPTR worsening, i.e. cell-to-cell variations (which proved to play an important role in [12]) we characterized the timing jitter of 1×1 mm^2 SiPM #2 collimating the light with pinhole. We employed a $200 \pm 5\ \mu$m diameter pinhole, positioned near the detector and illuminating the center, and then a $10 \pm 1\ \mu$m pinhole, illuminating only one cell in the central region. The dimensions and tolerances are given by manufacturer and they are made of stainless steel.

The SPTR obtained with and without pinholes varies of only few picoseconds. This small difference does not explain the 25 ps difference between 1×1 mm^2 SiPM and single cell. Therefore, the cell-to-cell uniformity proved to be very good in this device and performance variations among cells do not represent an important limiting factor for time resolution. This confirms also the results obtained in [21] on SiPMs from an old FBK production run.

C. Measurements at $\lambda = 850$ nm

We measured single-photon time-resolution of 1×1 mm^2 SiPM #2 and single cell #3 at infrared wavelength, with the same setup (without the second harmonics generator). In this condition part of the photons are absorbed in the substrate and have to diffuse towards the depleted region to be able to trigger an avalanche (thus with delay with respect to photons absorbed in depleted region). As shown in the inset of Fig. 12, this gives an long tail after the main peak in the timing response, with a time constant in the order of few nanoseconds (much bigger than the one in Fig. 6). The amplitude of the tail, normalized to the one of the main peak reduces increasing the excess bias. This could likely be because the epitaxial layer is not fully depleted at breakdown voltage and the depleted region gets bigger increasing excess bias: it reduces the amount of avalanches triggered by diffused-carriers with respect to carriers absorbed inside the depleted region.

Timing jitter FWHM at $\lambda = 850$ nm is higher than with the blue-light. For the 1×1 mm^2 SiPM it is about 500 ± 9 ps at low excess biases (where the tail amplitude is very high) but it reduces to about 115 ± 4 ps at 7.5 V (compared to ~ 80 ps at 425 nm). For the single cell, timing jitter is 53 ± 2.5 ps at 7 V of excess bias. Interestingly, the Gaussian fits at the two
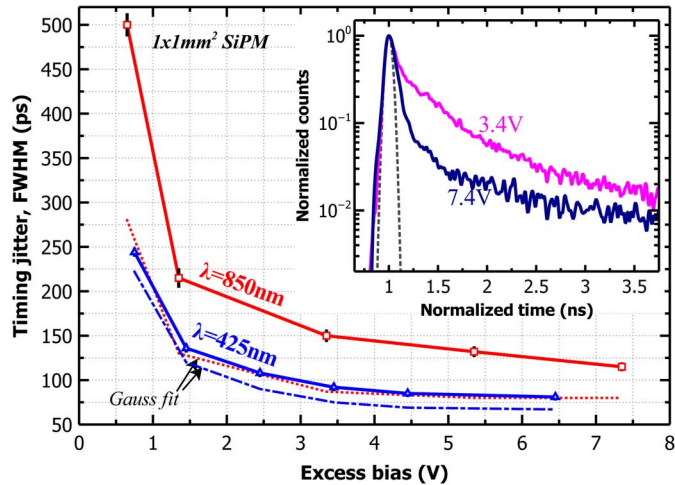
This article has been accepted for inclusion in a future issue of this journal. Content is final as presented, with the exception of pagination.

ACERBI *et al.*: CHARACTERIZATION OF SINGLE-PHOTON TIME RESOLUTION: FROM SINGLE SPAD TO SILICON PHOTOMULTIPLIER 7

Fig. 12. Timing jitter FWHM of 1×1 mm^2 SiPM #2 as a function of excess bias, at $\lambda = 425$ nm and $\lambda = 850$ nm. Dashed lines are the FWHM values of Gaussian fits, for both wavelengths. The inset shows two examples, at two biases, of timing responses at $\lambda = 850$ nm.
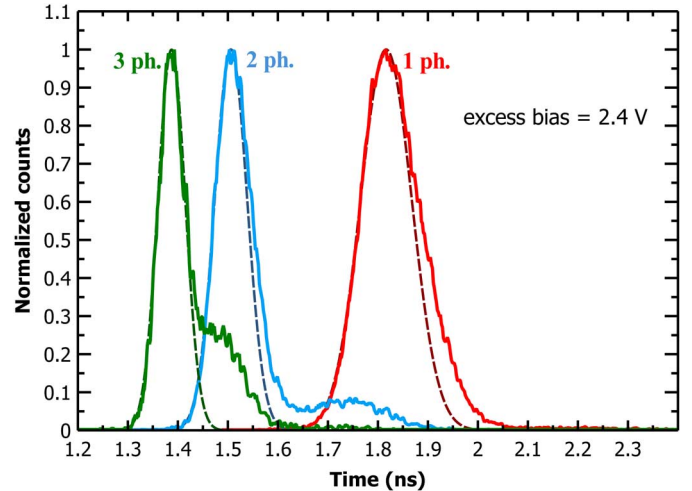

Fig. 13. Timing response acquired discriminating the events when 1 photon, 2 ph. or 3 ph. (of the laser pulse) trigger the SiPM (#1). Dashed lines are Gaussian fits. (The average Count rate was 0.77 counts per laser pulse).
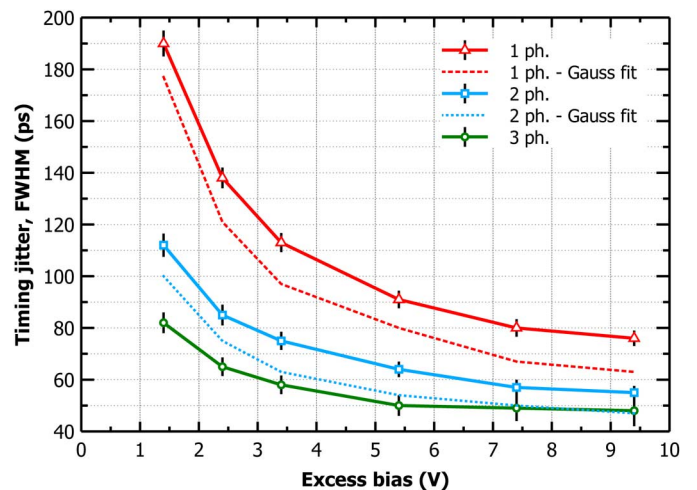
TABLE I
LOWEST MEASURED SINGLE-PHOTON TIMING JITTER (FWHM) FOR DEVICES TESTED IN THIS WORK

Device	Production run	DCR at 5V (Hz)	λ (nm)	Best SPTR (FWHM) (ps)
50-μm SPAD	#1	<100	425	48 ±2
50-μm SPAD	#3	>10·10^3	425	43 ±2
			850	53 ±2.5
1x1 mm^2 SiPM	#1	~90·10^3	425	76 ±2.5
1x1 mm^2 SiPM	#2	~600·10^3	425	81 ±2.5
			850	115 ±4
3x3 mm^2 SiPM	#1	~800·10^3	425	178 ±9

Fig. 14. 1-photon, 2-photons and 3-photons timing jitter of 1×1 mm^2 SiPM #1, as a function of the excess bias.

wavelengths are quite similar indicating that the tail is causing the timing jitter deterioration.

In conclusion, the lowest timing jitters, at the two wavelengths for the different devices, are summarized in Table I. For the 50-μm square cells the time resolution is lower than 50 ps at $\lambda = 425$ nm (between 44 ps and 48 ps) and it grows of about 10 ps at $\lambda = 850$ nm. 1×1 mm^2 SiPMs have a worse single-photon time resolution, of about 80 ps at 425 nm, and at 850 nm it increases of about 35 ps, reaching about 115 ps. A similar difference has been measured on AdvanSiD 1×1 mm^2 SiPM in [17].

V. TIME RESOLUTION AT INCREASING LIGHT INTENSITY

We also measured the time-resolution of 1×1 mm^2 SiPM #1 when triggered by more than one photon, i.e. when two or three avalanches are triggered at the same time in different cells. One difference between the single-photon and the two-photon cases is the higher signal amplitude: with two fired cells the signal has double amplitude and the crossing time of a given threshold voltage will happen slightly sooner. Moreover, as reported in [20], the electronic noise contribution in SPTR reduces approximately with the number of photons, whereas the intrinsic resolution reduces with the square root of the number of photons, because of the photoelectron statistics [7], [21]. In the present case (1×1 mm^2 SiPM #1), already with 2 photons the intrinsic

resolution became dominant, so square root dependence is expected.

Fig. 13 shows an example of timing response curves acquired simultaneously discriminating the case of 1, 2, or 3 photons. Peak position moves to shorter times and the FWHM of the curve reduces, increasing the number of photons. Moreover, the tail after the main peak reduces. The plot in Fig. 14 summarizes the timing jitter measured at different excess biases. The best values, at the highest excess bias, are 76 ps, 55 ps and 47 ps (all FWHM) for one, two and three photons, respectively. This trend is in agreement with the photoelectron statistics, even though the time resolution with 3-photons tends to saturate at high biases.

An interesting aspect is the anomalous second peak that emerges in the two and three photons timing responses. It gets bigger increasing the number of photons and its position is delayed, closer to the main peak of the histogram obtained with one photon less. We also see that it gets bigger when excess bias is increased. These characteristics suggest that it could be related to the optical crosstalk between cells of the silicon
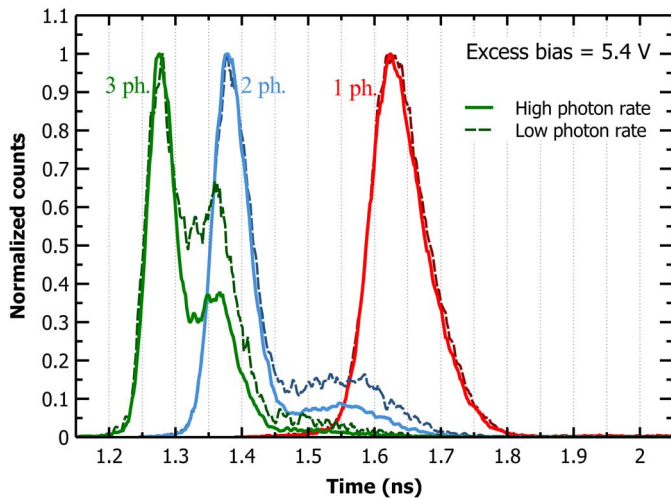
This article has been accepted for inclusion in a future issue of this journal. Content is final as presented, with the exception of pagination.

8 IEEE TRANSACTIONS ON NUCLEAR SCIENCE

Fig. 15. Timing responses acquired discriminating 1 photon, 2 photons or 3 photons events, on 1×1 mm^2 SiPM #1, in case of an average detection rate of 1.8 or 0.91 counts per laser pulse.

Fig. 16. Gauss fittings on different peaks of timing responses acquired discriminating 1 photon, 2 photons or 3 photons events, on 1×1 mm^2 SiPM #1, at 7.4 V of excess bias.

photomultiplier. As an example, when two photons are detected by the SiPM, they trigger two avalanches in the respective cells, emitting secondary photons; one of these photons can trigger an avalanche in a third cell and the resulting output current is three times the single-cell current. Since we discriminate the number of detected photons based on signal amplitude, this is considered among the three-photon events, but it was generated by two photons. Thus, it has not the arrival statistics typical of the 3-photon events.

To confirm this hypothesis we acquired timing histrograms at two different light intensities, keeping the same setup and detector conditions. As shown in Fig. 15, when the average number of photons per pulse is lower, the second peak has higher amplitude. Indeed, with a low photon rate, the probability that a pulse with amplitude of three fired-cells is generated by two photons and a crosstalk is higher than the case of three detected photons. Increasing the average number of photons, since the crosstalk probability depends only on the detector operating condition (not the photon flux), the probability of a three-photon event increases with respect to the probability of a two-photon with a crosstalk, and the second peak is reduced.

We also plot the curves on logarithmic axis, as shown in Fig. 16 at 7.4 V of excess bias. The secondary peak in the 2-photon curve is likely due to 1-photon plus 1-crosstalk events, whereas the secondary peak in the 3-photon curve by 2-photon plus 1-crosstalk event, and the third peak by 1-photon plus 2-crosstalk events. These three anomalous peaks appear in the curves at all excess biases, but with different amplitudes and widths. The widths of the Gaussians fit on the third peak of the 3-photon curve and the second peak of the 2-photon curve are very similar (at all biases), because they are both related to the 1-photon event statistics. However, they are larger than the 1-photon curve and this is probably caused by an additional spread in the first-avalanche build-up, which happens before the crosstalk events. For example, with 3.4 V, the Gaussian
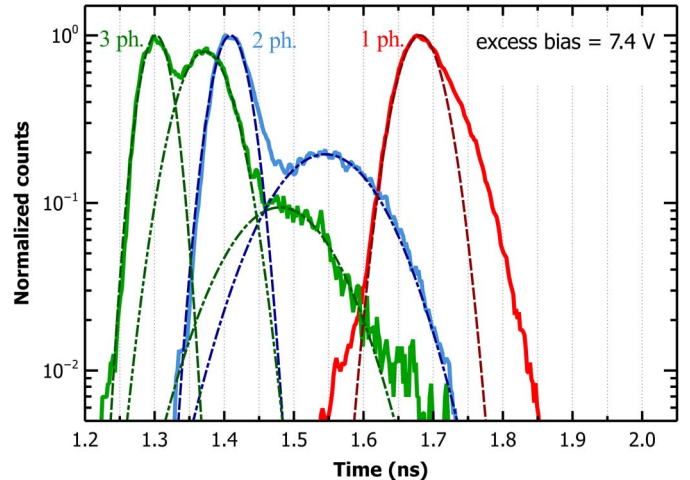
fitting on 1-photon curve has a FWHM of 94 ps, the one fitting the second peak of 2-photon curve has a FWHM of 177 ps, as well as the fitting on the third peak of the 3-photon curve; with 7.4 V, the fitting on 1-photon curve has a FWHM of 68 ps, whereas the fitting on the second peak of the 2-photon curve ~ 165 ps. In both cases the deconvolution gives a value of about 150 ps.

The left shift of the peaks position, in the histogram, of the 3-photon curve, with respect to the 2-photon and the 1-photon curves, towards left, is probably due to the higher slope: the crossing time of a given threshold happens at earlier times.

Considering the small time distance between the main peak and the second or third peaks, it is more likely that the direct-crosstalk is the cause, rather than delayed crosstalk, which can have delays also in the nanosecond range. However, the estimated amount of events generating the second peak seems higher than the measured direct-crosstalk probability, thus further investigation and analysis are required to understand if these peaks are due to direct crosstalk and/or to the very initial part of fast delayed crosstalk events.

Anyhow, this is an important limitation when we want to characterize the time resolution in response to a moderately-high number of photons (e.g. Cherenkov radiators), since crosstalk becomes more and more important and distorts the acquired timing response. This behavior could also be related to what is called "delayed events" in [17].

Finally, we tested the timing jitter of 1×1 mm^2 SiPM #2 with an increasing number of detected photons. As shown in Fig. 17, keeping the excess bias relatively low (1.4 V of excess bias), thus limiting the crosstalk probability (direct crosstalk probability is $\sim 6\%$), we characterized the timing jitter FWHM up to 25 photons by measuring the 3 point at a time. The plot follows a decreasing trend with the square root of photon number (note that points at 15, 20 and 25 photons were acquired with a little higher light intensity). Instead, increasing the bias to just 2.4 V (direct crosstalk probability is $\sim 12\%$), the SPTR lowers
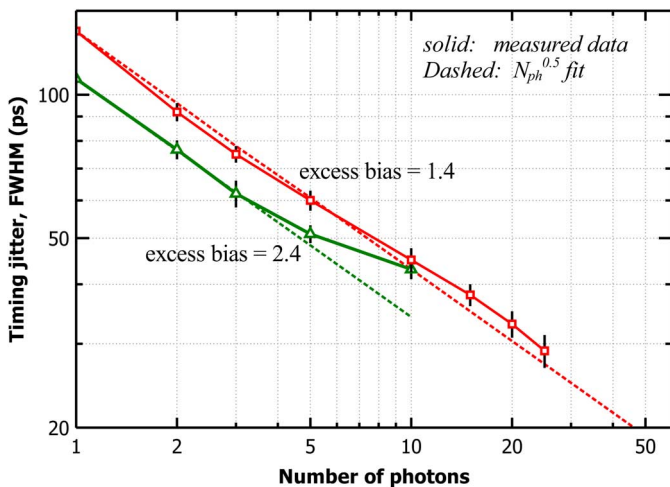
This article has been accepted for inclusion in a future issue of this journal. Content is final as presented, with the exception of pagination.

ACERBI *et al.*: CHARACTERIZATION OF SINGLE-PHOTON TIME RESOLUTION: FROM SINGLE SPAD TO SILICON PHOTOMULTIPLIER 9

Fig. 17. Timing jitter, measured with 1×1 mm^2 SiPM #2, as a function of the number of detected photons, for two excess biases.

of about 15 ps, but the curves significantly deviate from the trend with 10 photons, reaching a value 45 ps.

VI. CONCLUSIONS

We characterized the performance of new low-noise RGB silicon photomultipliers produced at FBK, with n-on-p implant technology, focusing on the single-photon time resolution, analyzing what are its main limiting factors. They show a peak detection efficiency, in the green wavelength region, of about 33%, with 6.5 V of excess bias (including the fill factor of $\sim 45\%$) and a very low noise, among the lowest reported: DCR is about $1 \cdot 10^5$ cps/mm^2 at 6 V of excess bias (at $20°C$).

We characterized the single-photon time resolution (SPTR) of 1×1 mm^2 and 3×3 mm^2 SiPMs (same cell size): timing jitter is lower than 80 ps FWHM, at $\lambda = 425$ nm, for the 1×1 mm^2 SiPMs with excess biases higher than 7 V, and it increases of about 35 ps when illuminated at $\lambda = 850$ nm, due to a slow tail in the timing histogram. For the 3×3 mm^2 SiPM we measured 180 ps at 6.5 V of excess bias ($\lambda = 425$ nm). These are among the best SPTR values reported in literature for SiPMs.

To understand the contributions to time resolution we characterized SPTR of SiPMs with light collimated by pinholes, and also the SPTR of a SPAD identical to single cells composing the SiPMs, which have a time jitter lower than 50 ps FWHM. By analyzing the average signal shape, we observed that SPTR in SiPMs is dominated by electronic noise contribution and the degradation of SPTR, increasing the device dimension, is principally due to the slower rising edge of the signal (because of the higher capacitance). We extrapolated the "intrinsic" time resolution of the single-cell which is the same for the three devices.

Effect of dark count is almost negligible in this low-noise SiPMs, thus, a better front-end electronics or a more prompt single-cell signal is necessary to improve SPTR.

Finally, we also characterized the time resolution of SiPMs at increasing light intensity. We found that the optical cross-talk between cells have an important effect and it can limit the minimum achievable time resolution given by the SPTR divided by

the square root of the number of photons. It must be considered and reduced to improve timing performances.

REFERENCES

[1] D. Renker, "Geiger-mode avalanche photodiodes, history, properties and problems," *Nucl. Instrum. Methods Phys. Res. A*, vol. 567, pp. 48–56, 2006.

[2] D. W. Townsted, "Multimodality imaging of structure and function," *Phys. Med. Biol.*, vol. 53, pp. R1–R39, 2008.

[3] W. W. Moses, "Recent advances and future advances in time-of-flight PET," *Nucl. Instrum. Methods Phys. Res. A*, vol. 580, pp. 919–924, 2007.

[4] G. Muehllehner and J. S. Karp, "Positron emission tomography," *Phys. Med. Biol.*, vol. 51, no. 13, p. R117, 2006.

[5] S. Surti, A. Kuhn, M. E. Werner, A. E. Perkins, J. Kolthammer, and J. S. Karp, "Performance of Philips Gemini TF PET/CT scanner with special consideration for its time-of-flight imaging capabilities," *J. Nucl. Med.*, vol. 48, no. 3, pp. 471–480, 2007.

[6] S. Seifert, H. T. van Dam, and D. R. Schaart, "The lower bound on the timing resolution of scintillation detectors," *Phys. Med. Biol.*, vol. 57, pp. 1797–1814, 2012.

[7] S. Gundacker *et al.*, "SiPM time resolution: From single photon to saturation," *Nucl. Instrum. Methods Phys. Res. A*, vol. 718, pp. 569–572, 2013.

[8] M. G. Albrow, H. Kim, S. Los, E. Ramberg, A. Ronzhin, V. Samoylenko, H. Wenzel, and A. Zatserklyaniy, "Quartz Cherenkov Counters for Fast Timing: QUARTIC," *J. Instrum.*, vol. 7, Oct. 2012.

[9] A. Gamal, B. Paul, C. Michael, H. Roland, M. Johann, O. Herbert, and S. Ken, "Application of Geiger-mode photosensors in Cherenkov detectors," *Nucl. Instrum. Methods Phys. Res. A*, vol. 639, no. 1, pp. 107–110, May 2011.

[10] A. Gamal, B. Paul, M. Johann, and S. Ken, "Silicon photomultiplier timing performance study," *Nucl. Instrum. Methods Phys. Res. A*, vol. 652, no. 1, pp. 528–531, Oct. 2011.

[11] Q. Peng, W.-S. Choong, and W. William Moses, "Evaluation of the timing properties of a High Quantum Efficiency Photomultiplier Tube," *IEEE Trans. Nucl. Sci.*, vol. 60, no. 5, pp. 3212–3219, Oct. 2013.

[12] T. Nagano, K. Sato, A. Ishida, T. Bada, R. Tsuchiya, and K. Yamamoto, "Timing resolution improvement of MPPC for TOF-PET imaging," in *Proc. IEEE Nuclear Science Symp. and Medical Imaging Conf.*, 2012, pp. 1577–1580.

[13] N. Serra, A. Ferri, A. Gola, T. Pro, A. Tarolli, N. Zorzi, and C. Piemonte, "Characterization of new FBK SiPM technology for visible light detection," *J. Instrum.*, vol. 8, Mar. 2013.

[14] C. Piemonte, A. Ferri, A. Gola, A. Picciotto, T. Pro, N. Serra, A. Tarolli, and N. Zorzi, "Development of an automatic procedure for the characterization of silicon photomultipliers," in *Proc. IEEE Nuclear Science Symp. and Medical Imaging Conf. Rec.*, 2012, pp. 428–432.

[15] M. Ahmed, B. Camanzi, and J. Matheson, "Characterization of silicon photomultipliers for time-of-flight PET," *Nucl. Instrum. Methods Phys. Res. A*, vol. 695, pp. 252–256, 2012.

[16] A. Lacaita, S. Cova, M. Ghioni, and F. Zappa, "Single-photon avalanche diode with ultrafast pulse response free from slow tails," *IEEE Electron. Device Lett.*, vol. 14, no. 7, pp. 360–362, 1993.

[17] V. Puill, C. Bazin, D. Breton, L. Burmistrov, V. Chaumat, N. Dinu, J. Maalmi, J. F. Vagnucci, and A. Stocchi, "Single photoelectron timing resolution of SiPM as a function of the bias voltage, the wavelength and the temperature," *Nucl. Instrum. Methods Phys. Res. A*, vol. 695, pp. 354–358, 2012.

[18] A. Gola, C. Piemonte, and A. Tarolli, "Analog circuit for timing measurements with large area SiPM coupled to LYSO crystals," in *Proc. IEEE Nuclear Science Symp. and Medical Imaging Conf.*, 2011, pp. 725–731.

[19] H. Spieler, "Fast timing methods for semiconductor detectors," *IEEE Trans. Nucl. Sci.*, vol. 29, no. 3, pp. 1142–1158, Jun. 1982.

[20] R. Vinke, H. Löhner, D. R. Schaart, H. T. Van Dam, S. Seifert, F. J. Beekman, and P. Dendooven, "Optimizing the timing resolution of SiPM sensors for use in TOF-PET detectors," *Nucl. Instrum. Methods Phys. Res. A*, vol. 610, no. 1, pp. 188–191, 2010.

[21] G. Collazuol *et al.*, "Single photon timing resolution and detection efficiency of the IRST silicon photo-multipliers," *Nucl. Instrum. Methods Phys. Res. A*, vol. 581, pp. 461–464, 2007.